# APPLICABILITY OF LEVEE FRAGILITY FUNCTIONS DEVELOPED FROM JAPANESE DATA TO CALIFORNIA'S CENTRAL VALLEY

Dong Youp Kwak[1]
Scott J. Brandenberg[2]
Atsushi Mikami[3]
Ariya Balakrishnan[4]
Jonathan P. Stewart[5]

## ABSTRACT

A fragility model for seismic deformations of levees was developed in a separate study using case history data from the Shinano River region of Japan (SRJ). In that model, levee fragility was shown to be principally related to ground motion intensity, geomorphology, and ground water level relative to the levee base. Our objective in this manuscript is to demonstrate the applicability of the developed fragility models for geotechnical conditions along urban levees in the Central Valley region of California (CVC). For this purpose, we compare SPT penetration resistance data (in the form of energy- and overburden-corrected blow counts) between regions for common soil types conditional on geology and topography. Among the geologic categories considered, arguably the most important is Holocene flood plain deposits, which comprise 38% of investigated sites in CVC and 97% in the SRJ. Within this geological unit, we find penetration resistance data for coarse-grained soils in the SRJ and CVC study regions to be similar, whereas for fine-grained soils the CVC sediments are stiffer. For two other geological units (Holocene basin and Pleistocene), both coarse- and fine-grained deposits in the CVC are stiffer than Holocene floodplain deposits. We also considered topographical conditions (elevation, ground slope and river gradient) as alternative means for sorting the data, with the general conclusion that such indicators are less capable than geology of describing variations of penetration resistance within the respective regions. The results provide insight into the relative vulnerability of levees in the two regions for given levels of ground motion amplitude.

## INTRODUCTION

Stewart et al. (2013) developed a fragility model for seismic deformations of levees along the Shinano River system in Japan (including tributaries) using a dataset of levee performance and related predictive parameters following two **M** 6.6 earthquakes from

[1] Doctoral Student, Department of Civil & Environmental Engineering, University of California, Los Angeles, CA 90095, duckkwak@ucla.edu
[2] Associate Professor and Vice Chair, Department of Civil & Environmental Engineering, University of California, Los Angeles, CA 90095, sjbrandenberg@ucla.edu
[3] Associate Professor, Department of Civil & Environmental Engineering, The University of Tokushima, Japan 770-8506, amikami@ce.tokushima-u.ac.jp
[4] Supervising Engineer, California Department of Water Resources, 1416 Ninth Street, Room #5106, Sacramento, CA 95814, ariya.balakrishnan@water.ca.gov
[5] Professor and Chair, Department of Civil & Environmental Engineering, University of California, Los Angeles, CA 90095, jstewart@seas.ucla.edu

2004 and 2007. This combination of levee system and earthquake event was selected because (1) the Japanese government recorded excellent post-event field performance data, (2) an extensive ground motion network permitted accurate spatial interpolation of shaking conditions, (3) geotechnical and geological information were available, and (4) the earthquake magnitudes are consistent with modal magnitudes controlling seismic hazard for urban levees in the California Central Valley. The developed levee fragility relations are a function principally of ground shaking amplitude, geomorphologic category, and elevation of the water table relative to the levee base. As examples, the fragility curves conditional on *PGA* and *PGV* are shown in Figure 1. Log-normal CDFs are adopted as functional forms of the fragilities, where the equation is as follows:

$$P = \Phi\left(\frac{\ln(PGA) - \mu}{\beta}\right) \tag{1}$$

where $P$ is the probability of being damaged, $\Phi$ is normal CDF operator, and $\mu$ and $\beta$ are moments of log-normal CDF (i.e., mean and standard deviation), respectively. The fragility functions conditional on other parameters in detail are provided in Stewart et al. (2013). We continue to work on developing fragility functions that utilize site-specific geotechnical inputs such as penetration resistance.

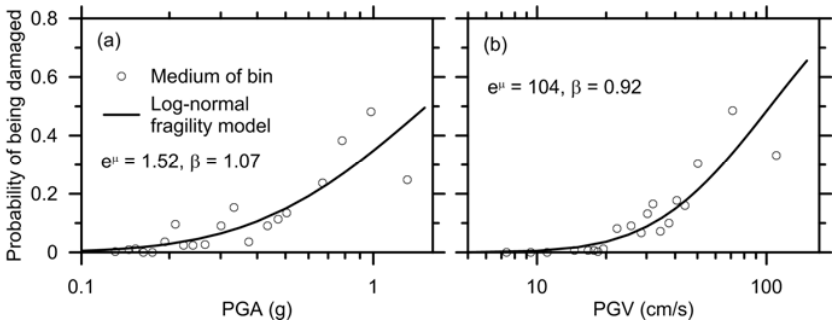


Figure 1. Fragility functions indicating probability of being damaged conditional on (a) *PGA* and (b) *PGV* (after Stewart et al, 2013).

The aforementioned fragility functions from the Shinano River region of Japan (SRJ) are potentially very useful for assessing the seismic response of levees elsewhere, but with a substantial caveat – are the geotechnical conditions in the study region comparable to those in the application region? We answer that question in this paper for the case of the study region being SRJ and the application region being the Central Valley of California (CVC).

This paper compares geotechnical conditions beneath levees in SRJ with those for urban levees in the CVC. Available data include penetration test measurements from 410 borings along the Shinano River and Uono River levee systems in Niigata, and 643 borings along rivers, creeks, bypasses, canals, and sloughs in the Central Valley. Some Central Valley levees are on the eastern margin of the Delta, but Delta levees resting atop peaty organic soil are not considered in this paper both because our focus is on urban levees and soil conditions comparable to those in the Delta are not present in SRJ. Our penetration resistance comparisons are conditioned on soil type, surface geology, ground slope, and river gradient.

## DATA SOURCES

Data utilized in this study include (1) penetration resistance measurements, (2) surface geology maps of various resolution, (3) elevation data of various resolution, and (4) streamgauge measurements.

### Penetration Resistance

Figure 2 shows the borehole locations of the study regions, and Table 1 indicates the name, length, and number of boreholes within each system. The total length of levees considered for the SRJ levee system is 166 km and the number of boreholes is 410, whereas the total length for CVC levee system is 358 km and the number of boreholes is 643. The scale of the map used in Figure 2 a to d is the same, which indicates that boreholes in CVC cover an area approximately three times broader than SRJ. The soil conditions beneath the levees are evaluated from boring logs that include standard penetration tests and other types of sampling.

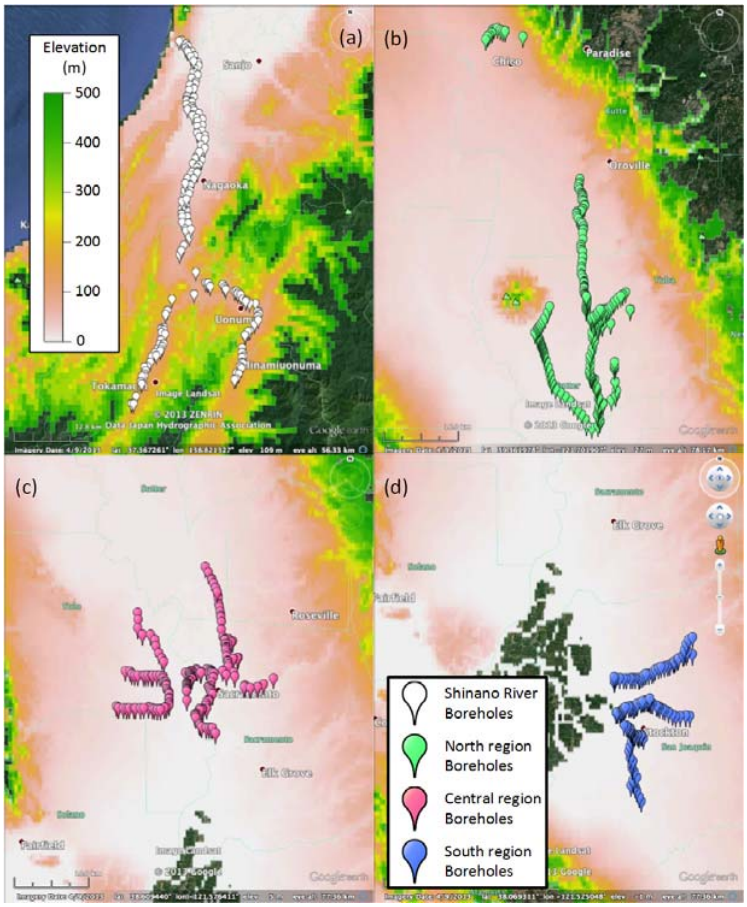


Figure 2. Google Earth maps showing borehole locations and Digital Elevation Map (DEM) from GTOPO30 with 30 arc second resolution for (a) the Shinano River region in Japan, (b) North, (c) Central, and (d) South regions in California's Central Valley.

Table 1. List of locations where levees present in this study. Region, river (or bypass, canal, or creek, etc.) name, length, and number of boreholes are indicated

| Region | | River (or bypass, canal, or creek, etc.) | Length (km) | Number of boreholes |
|---|---|---|---|---|
| Niigata, Japan | Shinano River system | Shinano River – Left-side | 59 | 177 |
| | | Shinano River – Right-side | 60 | 153 |
| | | Uono River – Left-side | 23 | 40 |
| | | Uono River – Right-side | 24 | 40 |
| | | Total | 166 | 410 |
| Central Valley | North | Feather River | 72 | 127 |
| | | Yuba River | 21 | 44 |
| | | Sutter Bypass | 28 | 34 |
| | | Wadsworth Canal | 7 | 10 |
| | | Mud Creek | 4 | 6 |
| | | Sycamore Creek | 7 | 6 |
| | | WPIC | 10 | 11 |
| | | Jack Slough | 4 | 23 |
| | | Total | 153 | 261 |
| | Central | Sacramento River | 27 | 51 |
| | | American River | 19 | 11 |
| | | Willow Slough Bypass | 12 | 17 |
| | | Yolo Bypass | 21 | 51 |
| | | Natomas East Main Drainage Canal | 27 | 36 |
| | | South Fork Putah Creek | 13 | 17 |
| | | Cache Creek Settling Basin | 9 | 5 |
| | | Total | 128 | 188 |
| | South | San Joaquin River | 27 | 84 |
| | | Calaveras River | 10 | 35 |
| | | Bear Creek | 25 | 43 |
| | | French Camp Slough | 3 | 15 |
| | | Mormon Slough | 12 | 17 |
| | | Total | 77 | 194 |

For SRJ, boring logs were either images or digitized versions obtained from the Shinano River Work Office (SWO) under the Ministry of Land, Infrastructure, Transport and Tourism (MLIT). This data includes layer descriptions according to a Japanese soil classification system, layer boundary depths, groundwater depths at various times, SPT penetration resistance (without energy or overburden corrections), and depths of SPT measurements. The soil classifications in the boring logs follow a system that is similar to the Unified Soil Classification System (USCS), in that it provides the soil type and the soil fines content in an approximate manner. The system uses three letters (JHPC, 2005):

1) First letter represents the major soil type comprising > 50% of the soil mixture by dry weight (G for gravel, S for sand, M for silt, C for clay, Pt for peat);
2) Second letter, as applicable, represents a minor soil type comprising 15-50% of the soil mixture by dry weight;

3) Third letter, as applicable, represents a sub-minor soil type comprising 5-15% of the soil mixture by dry weight.

For example, a material consisting of 67.5% gravel (G) and 22.5% sand (S), and 10% silt (M) would classify as GS-M.

For CVC, boring logs were either images or digitized versions obtained from the California Department of Water Resources (CDWR). The CVC soil types given in the boring logs according to the USCS (classified from formal index testing or visual inspection). The CVC boring logs were divided among the North, Central, and South regions shown in Figure 2.

We utilize data only within the foundation to 10 m depth because the potential for earthquake-induced levee damage is mostly contained within the near surface soils. The levees themselves do not contribute significantly to seismic instabilities because they are most often unsaturated (i.e., these flood control levees are most often not retaining water). Furthermore, we exclude refusal (i.e., N>50) and zero blow count (N=0) cases from consideration to focus on soil conditions for which SPT blow count is a reasonable indicator of soil strength. Figure 3 shows the percentage of soil type (i.e., rock, gravel, sand, silt, and clay) present in the SRJ and CVC systems. For SRJ, the major soil types are coarse-grained sands and gravels. Fine-grained soils comprise less than 20% of soil types. Peats are rarely encountered in the study area (0.3%). For CVC, approximately 60% of the foundation materials are fine-grained soils (silts and clays). Higher proportions of fine-grained soils are present in the CVC region than in the SRJ region.

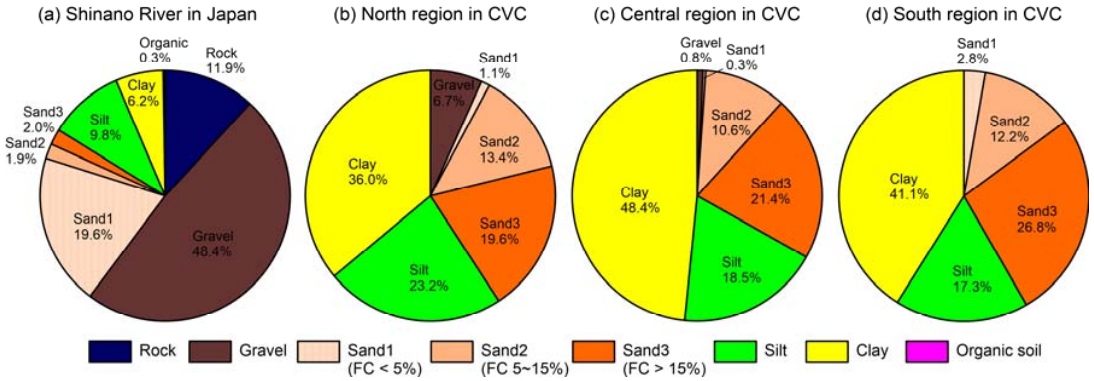


Figure 3. Percentage of foundation materials to 10 m depth for primary soil types in (a) Shinano River system in Japan and (b) North, (c) Central, and (d) South regions in Central Valley of California. Sand is separated further according to fines content (< 5%, 5 ~ 15%, and > 15%).

The practices and tools to carry out SPT penetration tests differ between Japan and California. To compare the same metrics between these regions, we compare values of $(N_1)_{60\text{-}CS}$ for coarse grained soils and $(N_1)_{60}$ for fine grained after correcting for hammer energy efficiency, overburden pressure, and fines content. For the borehole data in SRJ, hammer efficiency is assigned for each boring based on hammer type and drop mechanism, which is described in the electronic version of the boring logs as having four

categories: automatic drop hammer, semi-automatic drop hammer, mechanical trip device (referred to as tonbi) that is nearly free-fall, and the rope-pulley method (JHPC, 2005). We assigned energy efficiencies of 78% to automatic, semi-automatic, and tonbi methods and 67% to the rope-pulley method, which are average values for those methods (Seed et al., 1985). For CVC, hammer efficiencies for boreholes are directly provided in electronic versions of boring logs (68% ~ 88%). Effective stresses at SPT locations are calculated as total stress minus pore water pressure. Unit weights for total stresses were computed assuming typical values in engineering practice, e.g., moist unit weights $\gamma_t$ of rock, gravel, sand, silt, and clay above the water table are taken as 24, 21, 19, 16, and 14 kN/m$^2$, and saturated unit weights $\gamma_{sat}$ of rock, gravel, sand, silt, and clay are taken as 25, 22, 20, 18, and 16 kN/m$^2$, respectively (NAVFAC, 1986). The effective stress caused by levee fill was also considered. Water pressures were computed from water table depths assuming hydrostatic conditions. When available, groundwater elevation reported in boring logs was used. Groundwater elevation was not reported for some CVC borings, in which case we assume that the water table is 3, 4, and 2 m below the levee base for North, Central, and South regions for Holocene deposits (i.e., Holocene floodplain and basin deposits), respectively. For Pleistocene deposits, 8, 10, and 6 m are used. Those numbers are medians of measured ground water depths for each case.

As shown in Figure 3, the coarse-grained soil in CVC contains more fines content than SRJ, which affects liquefaction resistance. To account for this fines content difference on the comparison of penetration resistance for coarse-grained soils, we estimate the clean sand equivalent $(N_1)_{60\text{-}CS}$ for both regions using the following equation (Idriss and Boulanger, 2008):

$$\left(N_1\right)_{60-CS} = \left(N_1\right)_{60} + \exp\left(1.63 + \frac{9.7}{FC + 0.01} - \left(\frac{15.7}{FC + 0.01}\right)^2\right) \quad (2)$$

where *FC* is fines content in percent. For SRJ, the fines correction was insignificant, whereas for CVC, the blow counts increased by 4 to 5 on average.

## Geologic or Geomorphic Conditions

High resolution geologic maps (i.e., 1:24,000 to 1:62,500) were utilized to assign surface geology conditions at the location of each boring log. We found that low-resolution maps (i.e., 1:200,000) are inadequate to capture the fluvial deposits adjacent to major rivers, and incorrect characterization arises from the low-resolution maps in many cases. For the SRJ system, we use high resolution geomorphic maps from the Geospatial Information Authority of Japan (GSI, 2013) under MLIT. These are the same maps used by Stewart et al. (2013) to characterize surface geology for the fragility functions. For the CVC system, we use surface geology maps by the U.S. Geological Survey (USGS). Table 2 shows map resources, geologic units for CVC and geomorphic descriptions for SRJ, and number of boreholes for each group. The geomorphic classification system in the MLIT maps is different from the surface geology designations in the USGS maps. We adopt the USGS designation for the purpose of comparing blow counts from the SRJ and CVC regions because the geomorphic categories used in the MLIT maps are not available for the CVC

region. Based on the understanding of unit descriptions available from high resolution USGS maps, we group geologic units as (1) Holocene floodplain deposit, (2) Holocene basin-deposit, and (3) Pleistocene deposit. Most of the SRJ borings (97%) lie within Holocene floodplain deposits of the Shinano and Uono Rivers. The CVC borings often lie within Holocene floodplain deposits for levees along rivers, but also lie within Holocene basin-deposits and Pleistocene deposits adjacent to creeks, bypasses, canals, and sloughs.

Table 2. List of high resolution geomorphic or geologic maps for study regions in SRJ and CVC. Geomorphic descriptions for SRJ and geologic units for CVC assigned to each group are provided along with numbers of boreholes. $G_N$ and $G_L$ are used for symbols of geomorphic and geologic groups, respectively.

| Region | Resolution | Source | Geologic (or Geomorphic) groups | Number of boreholes |
|---|---|---|---|---|
| SRJ | 1:25,000 | GSI (2013) | $G_N$ 1. Alluvial Plain, Back Marsh, Old River Channel | 299 |
| | | | $G_N$ 2. High Embankment, Natural Levee, Old River Highland | 103 |
| | | | $G_N$ 3. Hill, Terrace | 8 |
| North in CVC | 1:62,500 | Helley and Harwood (1985) | $G_L$ 1. Holocene floodplain deposit (Qa) | 63 |
| | | | $G_L$ 2. Holocene basin deposit (Qb) | 43 |
| | | | $G_L$ 3. Pleistocene deposits (Qml, Qmu, Qrl, Qru, Qrb) | 155 |
| Central in CVC | 1:62,500 | Helley (1979) | $G_L$ 1. Holocene floodplain deposit (Qha) | 79 |
| | | | $G_L$ 2. Holocene basin deposit (Qhb) | 88 |
| | | | $G_L$ 3. Pleistocene deposits (Qml, Qmu, Qrl) | 21 |
| South in CVC | 1:24,000 | Atwater (1982) | $G_L$ 1. Holocene deposits (Qfp, Qpm) | 102 |
| | | | $G_L$ 2. Holocene and upper Pleistocene (Qcr) | 89 |
| | | | $G_L$ 3. Pleistocene deposit (Qm) | 3 |

## Topographic Conditions

Three different topographic parameters (elevation, ground slope, and river gradient) were utilized as conditioning variables because related parameters have been shown to correlate with soil stiffness previously (e.g., Wald and Allen, 2007; Ancheta et al., 2013). We utilize GTOPO30 that is a global digital elevation model (DEM) produced by the U.S. Geological Survey (USGS, 1996). The resolution of this DEM is a 30 arc seconds, which indicates approximately 1 km horizontal grid spacing. Although higher resolution DEMs are available through USGS Earth Resources Observation and Science (EROS) center [e.g., 1 arc second or 3 arc second DEMs by Shuttle Radar Topography Mission (SRTM); USGS, 2013], we choose 30 arc second DEMs because the smoother elevations are more representative of depositional conditions, and less influenced by man-made sources of topographic relief such as levees. The detailed technical procedures obtaining three topographic parameters (i.e., elevation, ground slope, and river gradient) are described following:

- Elevation: Elevation is directly taken from DEMs, where **R** (a computer language for statistical computing and graphics; RCT, 2013) is used to pull out the elevation ($v$) from GIS database (i.e., GTOPO30) downloadable from EROS center. A function "*raster*" in **R** reads the GIS database and forms a matrix (i.e., raster layer) where row and column indices and cell values are analogous to longitude ($x$), latitude ($y$), and $v$. This raster layer is converted to a three-column matrix of $x$, $y$, and $v$ by a function "*rasterToPoints*." We then find $v$ for target coordinates from the matrix, which are mapped in Figure 2 for study regions.
- Ground slope: The ground slopes are calculated using the "*terrain*" function (Hijmans, 2013) in **R**, which was originally utilized by Horn (1981). Ground slope in a grid is calculated utilizing elevations of 9 grids including the grid itself and adjacent 8 grids. Inputting the elevation raster layer from above and setting an option as slope [i.e., opt = c("slope")], the function *terrain* outputs a raster layer of ground slope. Again, we use *rasterToPoints* to find ground slopes at target points.
- River gradient: River gradient, which is a different metric from ground slopes, is calculated utilizing river distances and river water elevations. Actual river water elevations are used for SRJ (Stewart et al., 2013), but due to sparse river elevation data of CVC, DEMs at river locations are used for river elevations. River gradients are obtained from the rate of river elevation change by river distance. Only major rivers (i.e., Feather River, Sacramento River, American River, San Joaquin River and Calaveras River for CVC, and all regions in SRJ) are used for river gradient calculation because the distance for other water systems (creeks, canals, and bypasses) are man-made and may not reflect the natural environment at the time of deposition.

## COMPARISONS OF PENETRATION RESISTANCE

### Influence of Soil Type and Surface Geology

Figure 4 shows histograms of $(N_1)_{60\text{-}CS}$ values for Holocene floodplain deposits comprised of sand. We show these data first because this combination of soil type and geologic condition are expected to be the most susceptible to liquefaction, which is a significant driver of earthquake-induced levee damage. In this figure, *Num* indicates the number of blow counts that correspond to this condition, $X_m$ is the median value, and $\sigma_{\ln}$ is the standard deviation in natural log units. The distributions are similar, with the SRJ region exhibiting slightly lower median values than the CVC region.

Figure 5 shows histograms for sandy soil type Holocene basin deposits and Pleistocene deposits for the CVC region. Histograms for the SRJ region are not shown because so few borings were advanced in geological units other than Holocene floodplain deposits. The median values are significantly higher for these types of surface geology than for the Holocene floodplain deposits except South-Pleistocene deposit for which the number of data points is inadequate for comparison (*Num* = 9).

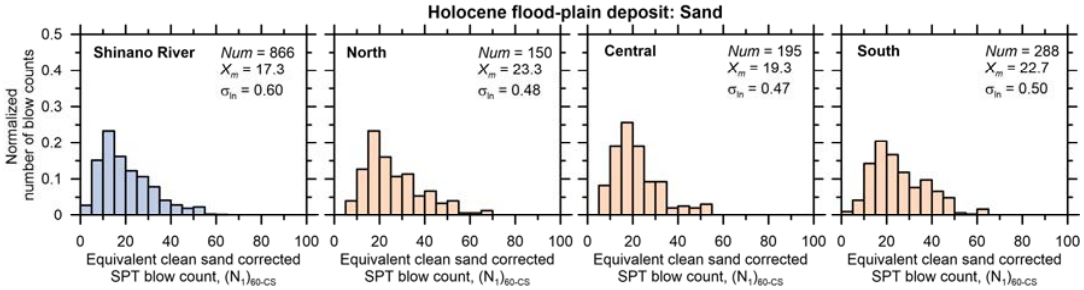


Figure 4. Histograms of energy- and overburden- corrected SPT blow counts for sandy soil modified by equivalent clean sand condition [i.e., $(N_1)_{60\text{-}CS}$; Idriss and Boulanger, 2008] in Holocene floodplain deposit. Median ($X_m$) and standard deviation ($\sigma_{\ln}$) in natural log unit are presented.

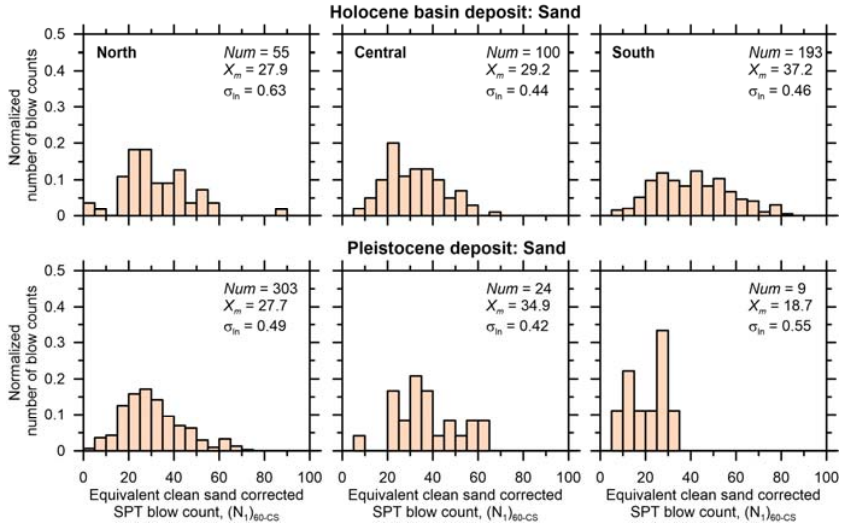


Figure 5. Histograms of energy- and overburden- corrected SPT blow counts for sandy soil modified by equivalent clean sand condition in Holocene basin deposits and Pleistocene deposits in the CVC region.

Figure 6 shows histograms of $(N_1)_{60}$ values for fine-grained (silt and clay) Holocene floodplain deposits. Fine-grained soils for the CVC regions are further separated according to the liquid limits (ML and CL vs. MH and CH), where the majority is low plasticity material (i.e., ML and CL). The plasticity information is unknown for the SRJ region. In Figure 6, histograms are shown as the same manner for sand (Figure 4), but use $(N_1)_{60}$ rather than $(N_1)_{60\text{-}CS}$. SPT blow count is known to be a poor indicator of the strength of plastic fine-grained soils, and we don't recommend correlating strength with blow count for these materials in design applications. Nevertheless, blow count provides a reasonable point of comparison for the different systems, and other more relevant data (e.g., vane shear, CPT) are unavailable for this comparison. For silt, the SRJ and CVC-Central distributions are the most similar, whereas the CVC-North and South regions exhibit a significantly higher median. For clay soil type, all CVC regions are significantly stiffer than SRJ.

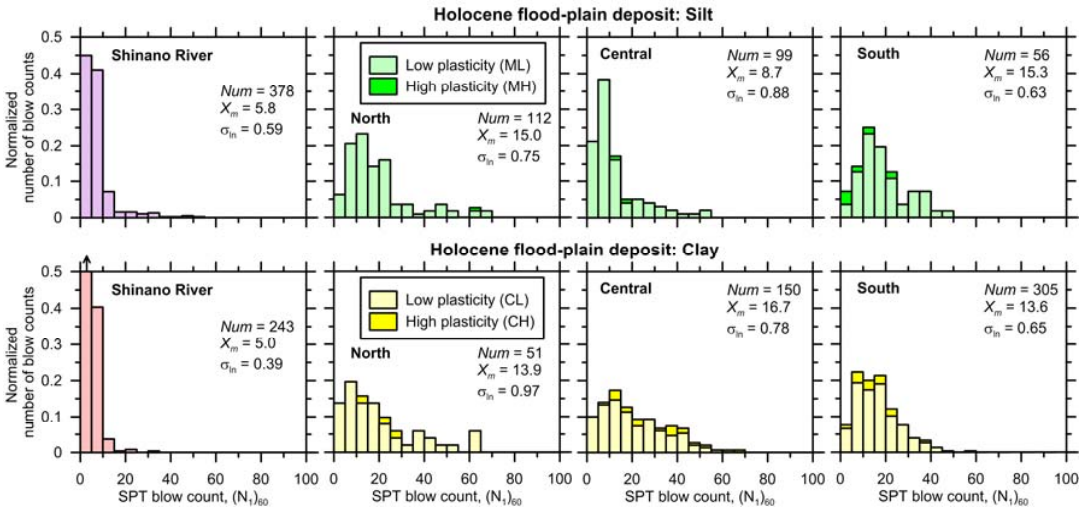


Figure 6. Histograms of energy- and overburden- corrected SPT blow counts conditional on geologic groups for silty and clayey soil. Median ($X_m$) and standard deviation ($\sigma$) in natural log unit are presented.

Figure 7 shows histograms of $(N_1)_{60}$ values for fine-grained soils having surface geology classifications of Holocene basin or Pleistocene. Again, the median values are significantly higher for these types of surface geology than for the Holocene floodplain deposits. Fine-grained materials for CVC with this geology type are again generally stiffer than fine-grained materials at SRJ.

Figure 8 shows log-normal probability density functions (PDFs) of blow count distributions for Holocene floodplain deposits for sand, silt and clay. We confirm that the distribution of sand is slightly higher for CVC, whereas the distributions of fine-grained soil types (silt and clay) for CVC are significantly higher than SRJ.

## Influence of Topography

Figure 9 shows the corrected SPT blow counts versus elevation, ground slope, and river gradient for Holocene floodplain deposits for the SRJ region and the three subregions in CVC. Linear fit lines with upper and lower 95% confidence intervals are also shown. The SRJ region shows very little correlation between penetration resistance and the considered topographic indicators. For CVC, sandy soils similarly do not show a correlation between $(N_1)_{60\text{-}CS}$ and topographic indicators, whereas $(N_1)_{60}$ for silt and clay increase with slope/elevation. Our interpretation is that topography does not provide a significant benefit for distinguishing sand stiffness across the SRJ and CVC datasets, but it does have some predictive power for silt and clay. Note that the topographic metrics are strongly correlated, which helps explain why the trends are similar for each metric.

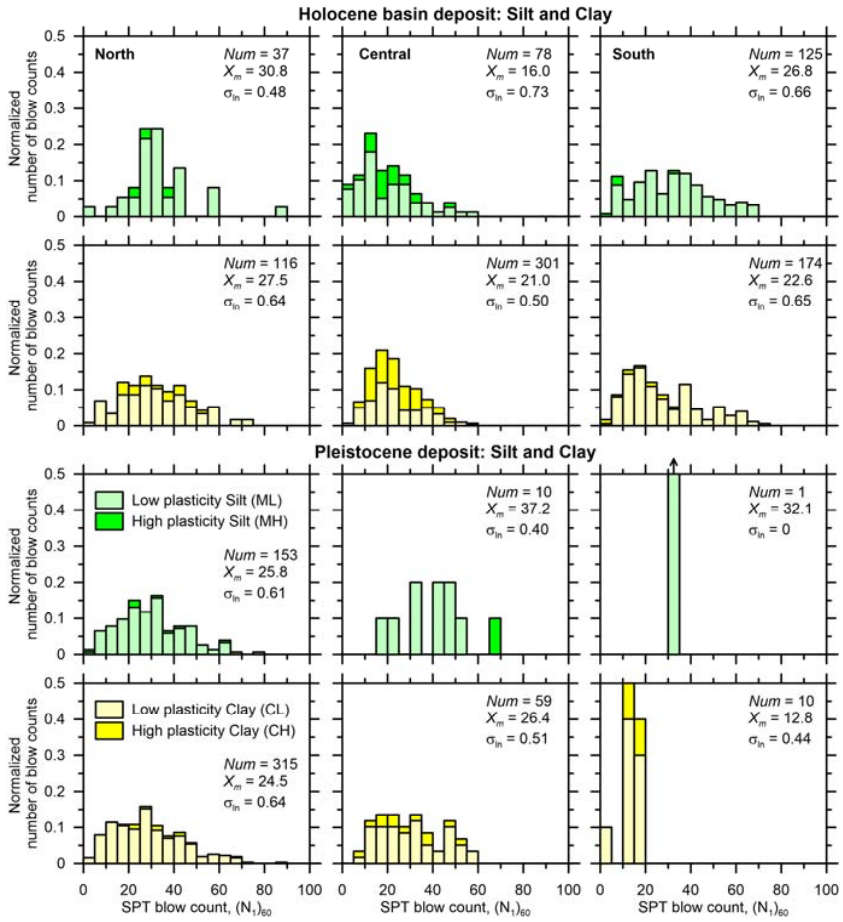


Figure 7. Histograms of energy- and overburden- corrected SPT blow counts for silty and clayey soil in Holocene basin deposits and Pleistocene deposits in the CVC region.

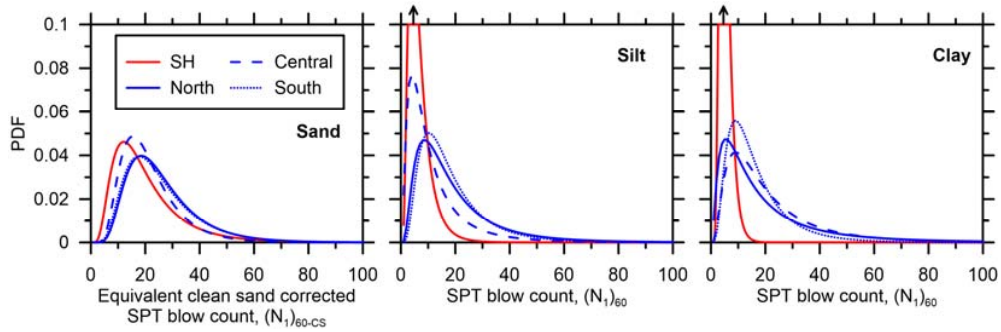


Figure 8. Probability density functions (PDF) for modified SPT blow counts [i.e., $(N_1)_{60\text{-}CS}$ for sand and $(N_1)_{60}$ for silt and clay] in Holocene floodplain deposits. SRJ and CVC-North, Central, and South regions are compared.

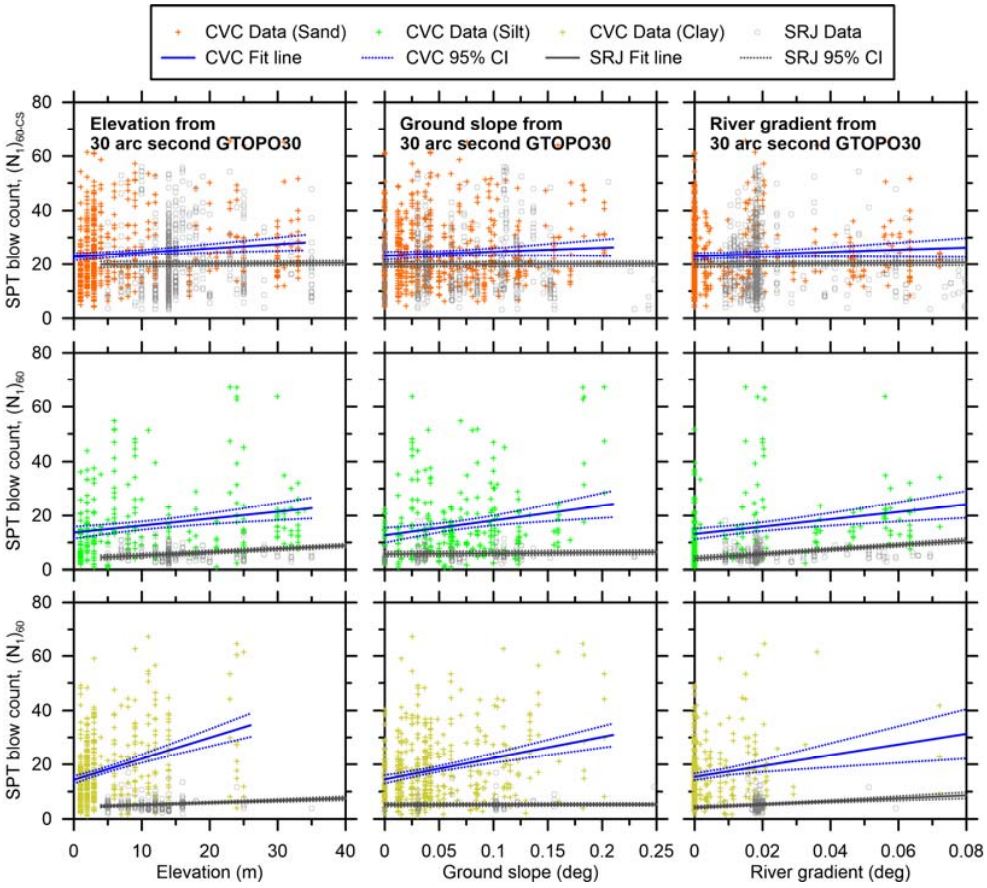


Figure 9. Elevation, ground slope, and river gradient vs. corrected SPT blow counts in Holocene floodplain deposits for SRJ and CVC including all subregions. Linear fits and 95% confidence intervals (CI) are shown.

## CONCLUSION

We compared penetration resistance measurements for borings along the Shinano and Uono River systems in Niigata, Japan with borings along urban levees in the Central Valley region of California. Sands in Holocene floodplain deposits were found to exhibit similar values of $(N_1)_{60\text{-}CS}$ in the two study regions. Holocene basin deposits and Pleistocene deposits in the Central Valley region exhibited higher median blow counts (such geology types were scarce in the Japanese borings). Topographic condition, represented by ground elevation, ground slope, and river gradient, had little predictive power when comparing sands between the two regions, whereas more significant trends were observed for silts and clays.

The purpose of comparing penetration resistance in these two regions was to ascertain whether fragility functions developed by Stewart et al. (2013) from the Japanese dataset could be applicable to the geological conditions in the Central Valley. Liquefaction was responsible for most of the heavily damaged levees in Japan, particularly for low to

moderate ground shaking levels that characterize Central Valley seismic hazard. Therefore we conclude that the fragility functions are applicable for coarse-grained Holocene floodplain deposits because the distributions of blow counts between the two regions were similar. Furthermore, this combination of soil type and geology is anticipated to significantly influence levee fragility. The fragility functions would be expected to over-predict seismic levee damage for fine-grained Holocene floodplain deposits, as well as Holocene Basin deposits and Pleistocene deposits encountered for Central Valley urban levees along creeks, bypasses, canals, and sloughs.

These conclusions are applicable only to Central Valley urban levees, and not to Delta levees that constantly impound water. Delta levees are anticipated to be much more susceptible to earthquake damage since the unengineered levee fills are saturated and often susceptible to liquefaction, and high groundwater elevation is associated with higher rates of levee damage (Stewart et al. 2013). Furthermore, the peat soils that underlie Delta levees are very scarce in the Japanese dataset, but may contribute to levee damage.

## ACKNOWLEDGEMENTS

This work was supported by California Department of Water and Resource (CDWR) under contract number 4600008849. This support is gratefully acknowledged. Any opinions, findings, and conclusions or recommendations expressed in this material are those of the authors and do not necessarily reflect those of the CDWR. We also acknowledge data providers, i.e., Ministry of Land, Infrastructure, Transportation and Tourism (MLIT), Shinano River Work Office (SWO), U.S. Geological Survey (USGS), and Geospatial Information Authority of Japan (GSI). Supportive work by undergraduate students Daniel La Franchi, Mark Bueno, and Nick Serra at UCLA is also acknowledged.

## REFERENCES

Ancheta, T. D., R. B. Darragh, J. P. Stewart, E. Seyhan, W. J. Silva, B. S. J. Chiou, K. E. Woodell, R. W. Graves, A. R. Kottke, D. M., Boore, T. Kishida, and J. L. Donahue (2013). PEER NGA-West 2 database. *PEER Report 2013/03*, Pacific Earthquake Engineering Research Center, Berkeley, CA.

Atwater, B. F. (1982). Geologic maps of the Sacramento-San Joaquin Delta, California. *U.S. Geological Survey Miscellaneous Field Studies Map MF-1401*.

Geospatial Information Authority of Japan (GSI) (2013). Geomorphological map for flood control use (in Japanese). Ministry of Land, Infrastructure, Transport and Tourism. (last accessed from http://www1.gsi.go.jp/geowww/lcmfc/lcmfc.html at June 2013)

Helley, E. J. (1979). Preliminary geologic map of Cenozoic deposits of the Davis, Knights Landing, Lincoln, and Fair Oaks quadrangles, California. *U.S. Geological Survey Open-File Report OF-79-583*.

Helley, E. J. and D. S. Harwood (1985). Geologic map of the Late Cenozoic deposits of the Sacramento Valley and northern Sierran Foothills, California. *U.S. Geological Survey Miscellaneous Field Studies Map MF-1790.*

Hijmans, R. J. (2013). raster: Geographic data analysis and modeling. *R package version 2.1-49*.

Horn, B. K. P. (1981). Hill shading and the reflectance map. *Proceedings of the IEEE*, 69, 14-47.

Idriss, I. M. and R. W. Boulanger (2008). *Soil liquefaction during earthquakes*. Earthquake Engineering Research Institute.

Japan Highway Public Corporation (JHPC) (2005). *Guidelines for Electronic Delivery of Surveys: Appendix of Geological Survey Part* (in Japanese).

Naval Facilities Engineering Command (NAVFAC) (1986). *Design Manual 7.01: Soil Mechanics*.

R Core Team (RCT) (2013). R: A Language and Environment for Statistical Computing. *R Foundation for Statistical Computing*, Vienna, Austria.

Seed, H. B., K. Tokimatsu, L. F. Harder, and R. M. Chung (1985). The influence of SPT procedures in soil liquefaction resistance evaluations. *Journal of Geotechnical Engineering*, 111(12), 1425–1445.

Stewart, J. P., D. Y. Kwak, S. J. Brandenberg, and A. Mikami (2013). Characterization of Seismic Fragility of Levees Using Filed Performance Data. *Project Report for California Department of Water Resources*, Civil & Environmental Engineering Dept., UCLA.

U.S. Geological Survey (USGS) (1996). GTOPO30.
(last assessed from: https://lta.cr.usgs.gov/GTOPO30 at October 2013)

U.S. Geological Survey (USGS) (2013). Earth Resources Observation and Science (EROS) Center. (last assessed from: https://eros.usgs.gov at October 2013)

Wald, D. J. and T. I. Allen (2007). Topographic slope as a proxy for seismic site conditions and amplification. *Bulletin of the Seismological Society of America*, 97(5), 1379-1395.